ROYAL SOCIETY
OF CHEMISTRY

PAPER

Check for updates

Evaluation of blood pressure using a flexible and wearable capacitive pressure sensor†

Bijender, [ab] Shubham Kumar, [ab] Amit Soni[ab] and Ashok Kumar*[ab]

In recent times, the high demand for flexible and wearable pressure sensors to monitor human health, particularly for patients afflicted with hypertension or high blood pressure (BP), has captured the keen interest of researchers. Capacitance-based flexible sensing devices offer real-time metrics regarding vital physiological parameters of the human body, such as BP and pulse rate (PR), thereby enabling the identification of cardiovascular complications. In this regard, we have developed a capacitive pressure sensor using polydimethylsiloxane (PDMS) and deionized water (DIW) and improved its key parameters by adding baking powder to PDMS-DIW. The sensor demonstrated excellent performance in static pressure measurements with a sensitivity of 0.021 Pa^{-1}, detection limit of 1 Pa, and response time of 100 ms. We further investigated its application in human BP monitoring. The sensor successfully captured the oscillometric waveform (OMW) for all 160 participants and demonstrated excellent performance in accurately measuring BP, meeting all criteria outlined as the universal standard when compared with the reference devices: OMRON BP device and the gold-standard mercury-based sphygmomanometer. Furthermore, the sensor accurately provided the PR and agreed well with the reference BP device. Therefore, the developed BP sensor can be a viable alternative to replace the pressure sensors in existing BP devices.

1. Introduction

BP refers to the force exerted by the blood on the arteries, which act as pathways for blood flow from the heart. It is measured based on two distinct values: systolic pressure (SP), which represents the highest pressure exerted during blood ejection, and diastolic pressure (DP), which reflects the lowest pressure experienced during heart relaxation. BP serves as a crucial physiological parameter as it provides insights into heart health, organ perfusion, and the overall hemodynamic stability of an individual.[1-3] Elevated BP or hypertension poses significant risks to human health as it is a prominent contributor to cardiovascular diseases, organ failure, and stroke.[5-7] Cardiovascular disease and the associated complications are considered the leading causes of death worldwide, claiming approximately 18 million lives in 2019 and accounting for nearly one-third of all fatalities.[4] Therefore, continuous BP monitoring is crucial for the early identification and treatment of disorders affecting the cardiovascular system.

The accuracy of BP monitoring devices highly depends on the quality of the pressure sensor used in it. In recent years, flexible pressure sensors have gained a lot of attention because of their wide range of applications, including artificial intelligence,[8,9] electronic skin,[10-12] human–machine interfaces,[13-15] and healthcare monitoring technology.[16-22] Despite the wide range of applications, flexible and wearable pressure sensors still have several challenges, which revolve around achieving quick response, high sensitivity, excellent operational stability, ultralow detection limits, and robustness.[23,24] To address these challenges, many researchers have demonstrated a variety of flexible pressure sensors based on piezoresistive,[25-27] capacitive,[28-32] piezoelectric,[33-35] and triboelectric[14,36-38] mechanisms, presenting high mechanical flexibility and superior key parameters (such as sensitivity, response/recovery time, working stability, and detection limit). They have also explored the applications of these sensors in flexible electronics, wearable devices, electronic skin, and human–machine interface devices.[18,39-43] In particular, among these sensors, capacitive pressure sensors have drawn significant attention for monitoring physiological signals because of their excellent key parameters and flexible nature, which allows them to form good contact with the human body without causing any harm to the skin. These advantages make capacitive sensors more suitable for applications in medical diagnostic systems compared with other pressure sensors.

Capacitive pressure sensors employ a dielectric layer positioned between two parallel electrodes to detect external pressure based on changes in capacitance.[44] To improve the performance of capacitive pressure sensors, researchers have explored various

[a]CSIR-National Physical Laboratory, Dr K. S. Krishnan Marg, New Delhi-110012, India. E-mail: ashok553@nplindia.org

[b]Academy of Scientific and Innovative Research (AcSIR), Ghaziabad-201002, India

approaches to modify the structure of the PDMS dielectric layer.[45,46] These modifications involve introducing pores,[47,48] creating wrinkled structures,[49] forming pyramids,[50] or transforming it into a sponge-like structure[51] to meet the requirements of specific applications. Among these methods, introducing pores in the dielectric layer has shown promising results toward enhancing sensor performance, particularly in monitoring human health.[52] The introduction of porosity provides the sensing device with high flexibility, which is crucial for attaching the sensor to the human body and accurately monitoring physiological activities. Researchers have employed different techniques to introduce porosity into the PDMS dielectric layer. For instance, DIW,[29] ammonium bicarbonate,[53] or a sugar cube template[32] can be utilized to create porosity in the dielectric layer. This advancement in sensor design and structure contributes to the development of more effective and reliable wearable devices for monitoring human health.

In this regard, this study describes the development of a highly sensitive and adaptable pressure sensor based on the capacitive phenomenon by employing PDMS as the dielectric layer. Baking powder and DIW were used to produce pores inside the PDMS layer to improve sensor performance and meet the needs of biological applications. The developed sensing device showed excellent performance in static pressure measurement, with a high sensitivity of 0.021 Pa^{-1}, an extremely low detection limit of 1 Pa, a quick reaction with a recovery time of 100 ms, and high operating stability. The aforementioned characteristics of the sensor demonstrate its potential in BP and PR monitoring, and the sensor could trace the oscillometric waveform very well for different health conditions. The maximum amplitude algorithm (MAA) approach, coded in the Python programming language, was used to determine the values of SP, DP, and mean pressure (MP) from the obtained OMW. A detailed analysis of several characteristic ratios led to the fixation of the SP and DP characteristic ratios. To clinically validate the sensor, a clinical trial was also carried out by including individuals from various age groups, and the error in BP readings with respect to a popular BP device (OMRON) and the gold-standard sphygmomanometer was calculated. The proposed sensor exhibited high accuracy and conformed to the international protocol established by the AAMI/ESH/ISO standard, which stands for Advancement of Medical Instrumentation, European Society of Hypertension, and International Organization for Standardization.[54]

2. Experimental section

2.1. Fabrication of the pressure sensor

As illustrated in Fig. 1(a), polymer PDMS and its curing agent (Dow Corning Sylgard 184) were mixed in a weight ratio of 10 : 1 using a magnetic stirrer. Baking powder with the chemical formula $NaHCO_3$ (purity 99.7%, Alfa Aesar) at 20 wt% and 1.5 mL DIW were added to the mixed solution and again stirred to make a homogenous mixture. The mixed solution was kept in a glass Petri dish and left at room temperature for 30 min to settle the mixture and eliminate air bubbles that unintentionally formed during the stirring process. The solution was then

heated for 30 minutes at 50 °C to make it dense and trap the water droplets inside the solution. Then, the hot plate temperature was raised from 50 to 120 degrees Celsius, and in the next 30 minutes, the baking powder disintegrated and emitted CO_2 gas while the water droplets evaporated as well. As a result of the simultaneous release of CO_2 gas and water evaporation, large porosity was introduced inside the cured PDMS layer, resulting in a sponge-like or foam-like layer, as shown in Fig. 1(b). The formed dielectric layer was carefully removed from the Petri dish and positioned between two flexible ITO/PET substrates (indium tin oxide coated poly (ethylene terephthalate)) to make electrical connections in subsequent investigations.

2.2. Structural characterization and measurements

The presence of porosity was examined using the top-view and cross-sectional pictures acquired using a scanning electron microscope (SEM) and the optical images captured with the aid of an Olympus microscope SZ61. The static pressure measurements were performed using an impedance analyzer (HIOKI 3532-50 LCR Hi-TESTER) at an applied frequency of 1 MHz and DC bias 1 V voltage. For static pressure measurements, a glass slide was used to fix the effective area of the designed sensor, and the dead weights with dimensions smaller than the glass slide were placed on the slide to exert external pressure on the sensor. A non-invasive blood pressure (NIBP) simulator was utilized to optimize the characteristic ratios to calculate the systolic and diastolic values and to find the relationship between capacitance (pF) and pressure (mmHg). To validate the accuracy of the developed sensor, a comparison was made with a mercury-based sphygmomanometer and an existing BP device (OMRON HEM-7130).

3. Results and discussion

3.1. Device fabrication and structural characterization

As mentioned in the experimental section, PDMS was used as the dielectric layer to construct the proposed sensing device. We had previously developed a sensing device by combining DIW with PDMS to improve performance. However, its performance was not good enough for monitoring BP and only provided a qualitative signature of the oscillometric waveform.[29] Therefore, in this investigation, baking powder was used to increase the porosity of the PDMS-DIW layer to boost its performance further at a large scale to obtain quantitative data while monitoring human BP. A blueprint of the entire fabrication procedure is given in Fig. 1(a). Fig. 1(b), which depicts the optical image of the highly porous PDMS layer, shows that the formed dielectric layer resembled a sponge or foam layer. The top-view and cross-sectional SEM images, as shown in Fig. 1(c) and (d), also corroborate the presence of porosity in the dielectric layer.

3.2. Functionality of the sensor during static pressure measurement

Static pressure measurements were conducted to determine the key features of the developed sensor, which are crucial for evaluating the performance of a sensor. The measurement process
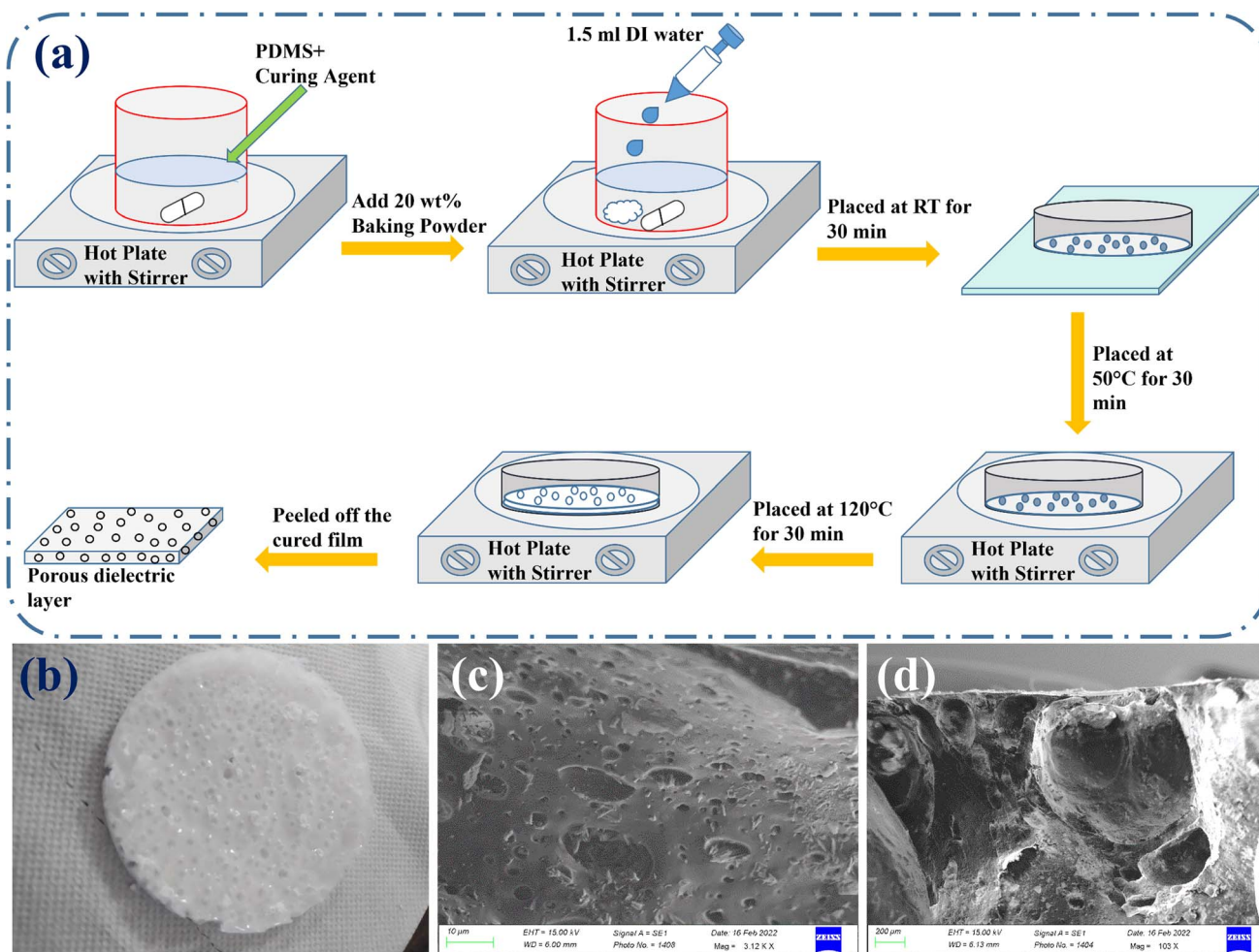
Fig. 1 The development of the porous dielectric layer. (a) Schematic representation of the fabrication approach. (b–d) The optical image, top-view, and cross-sectional SEM images of the fabricated porous PDMS layer.

involved placing the sensor on a rigid and insulating surface, the effective area of which was fixed using a glass slide. External pressure was applied using dead weights, and the fluctuations in sensor capacitance were recorded using an impedance analyzer. The sensor demonstrated remarkable sensitivity, detecting pressures as low as 1 Pa and exhibiting a relative capacitance shift of approximately 0.02%, as represented in Fig. 2(a). When the external pressure was gradually increased up to 111 kPa, it resulted in significant changes in sensor capacitance, with a relative difference of 90% at 111 kPa, as illustrated in Fig. S1.† To further analyze the variations in capacitance at different external pressures for better understanding, the applied pressure was divided into six pressure regions, as depicted in Fig. S1.† To evaluate the most vital parameter, *i.e.*, sensitivity, a graph correlating the relative capacitance shift with applied pressure was plotted, as demonstrated in Fig. 2(b).

Similarly, to assess the dependence of sensitivity on applied pressure, the applied pressure was categorized into various ranges. As per Fig. 2(b), the sensor exhibited the maximum sensitivity in the pressure range of 100–500 Pa, with a value of 0.021 Pa^{-1}. The sensor showed a linear response in various

pressure ranges, and the corresponding sensitivity values are also provided in Fig. S2.†

To check the operational or functional stability, the sensor was subjected to a 50 minute test at four different external pressures: 100 Pa, 500 Pa, 5 kPa, and 30 kPa. The sensor exhibited excellent operational stability with no output signal loss, as represented by Fig. 2(c). Furthermore, the response and recovery times of the sensor were determined to assess its potential use in biological applications. When pressure was applied, the sensor reacted quickly and returned to its initial state as the pressure was released. The designed sensing device showed an extremely low response and recovery time of 100 ms (as shown in Fig. 2(d)). This characteristic is suggestive of its viability in various biological applications. Overall, the developed sensing device showcases outstanding performance with improved vital parameters, highlighting its suitability for BP monitoring.

3.3. Application: monitoring of human BP

As seen in Fig. 3(a), several devices were used to monitor human BP, including an NIBP analyzer, an OMRON BP device,
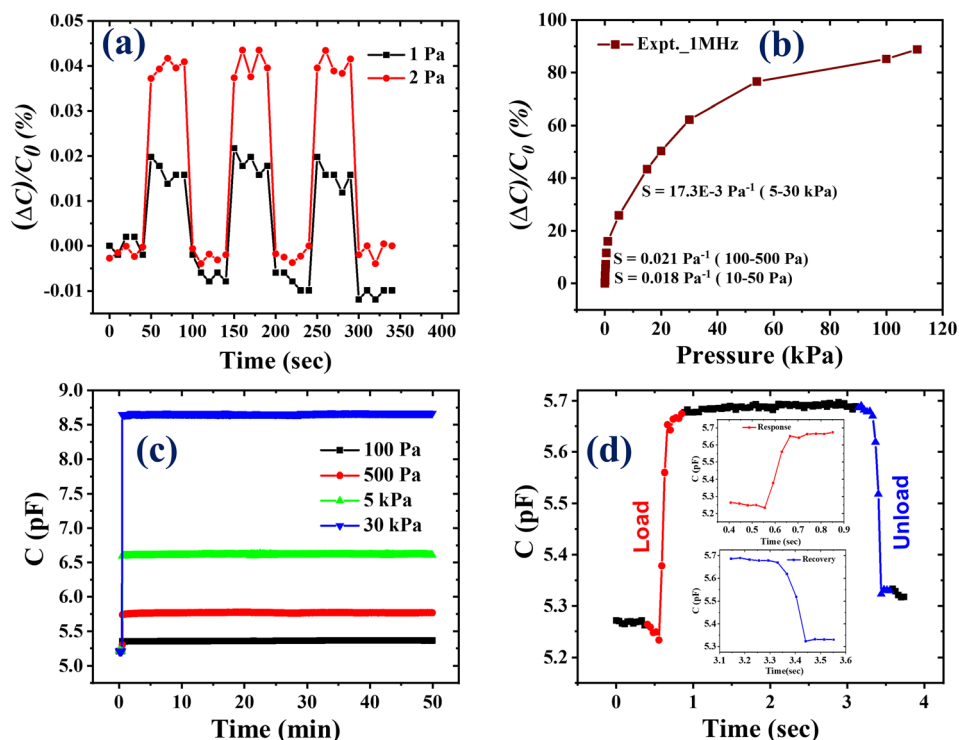
Fig. 2 The key factors related to the designed sensor. (a) An ultra-low detection limit of 1 Pa. (b) Capacitance variations with applied pressure. (c) The functioning stability of the developed sensor. (d) The reaction and recovery times of the sensor when it is loaded and unloaded.

a mercury-based sphygmomanometer with a stethoscope, and an impedance analyzer. Firstly, to establish the systolic and diastolic characteristic ratios required for evaluating the systolic pressure (SP) and diastolic pressure (DP) values from the oscillometric waveform envelope (OMWE), a comprehensive study was conducted using an NIBP simulator. Later, all other measurements were conducted on human volunteers as part of a clinical trial. In this study, the sensor was initially employed to measure blood pressure in the NIBP analyzer, which operates like an artificial heart and provides a stable pulse to the sensor based on predefined systolic pressure (SP) and diastolic pressure (DP) values. During this measurement, the sensor was positioned between a mandrel (representing an artificial hand) and a cuff connected to the NIBP analyzer, as shown in Fig. 3(b), which provides a visual representation of the experimental setup. An existing BP device was employed to apply pressure to the cuff and compare the result of the sensor to assess its accuracy. After extracting the OMW from the output signal and forming the OMWE, the MAA approach was used to calculate the SP and DP values using various characteristic ratios to the mean arterial pressure (MP) value: the range was 0.45 to 0.65 for SP and 0.60 to 0.80 for DP. The schematic representation of the MAA approach employed to calculate the BP value is explained in Fig. 3(d). The mean or average and standard deviation (SD) error were calculated for different systolic and diastolic ratios, as illustrated in Fig. 4. The analysis revealed that the average and SD error were minimal at a systolic ratio of 0.61 and a diastolic ratio of 0.62, as shown in Fig. 4(a) and (b). With the optimized systolic and diastolic characteristic ratios, the sensor

was further utilized in a clinical trial to validate its performance. The individuals involved in the clinical trial were from diverse age, weight, and height groups to ensure its applicability across different populations. The sensor accuracy was evaluated by comparing its results with the values obtained from an OMRON BP device and a mercury-based sphygmomanometer.

In the clinical trial, the developed sensing device was affixed to the mandrel; simultaneously, a cuff airbag, which was interconnected with another cuff encircling the upper arm of the participants, was placed over it. The reference devices, namely the OMRON BP device and the mercury-based sphygmomanometer, were connected at the common junction of the two cuff airbags. The pressure was applied within the cuff airbags using the BP device, while the pulse pressure emanated from the hands of the participants. The output of the developed sensor was measured by utilizing an LCR meter. The diagrammatic representation of this arrangement is depicted in Fig. 3(a), and an actual photograph is presented in Fig. 3(c). A total of 160 volunteers participated; the initial 130 subjects employed the OMRON BP device as the reference device, and for the remaining 30 individuals, the sphygmomanometer was used as the reference device. First, the 130 measurements performed with the BP device serving as the reference are discussed.

Out of 130 participants, 84 were male and 46 were female (over one-third); most were staff members of our laboratory (CSIR-National Physical Laboratory), and informed consent was obtained from all the volunteers in this study. Comprehensive information on participant age, height, and weight,
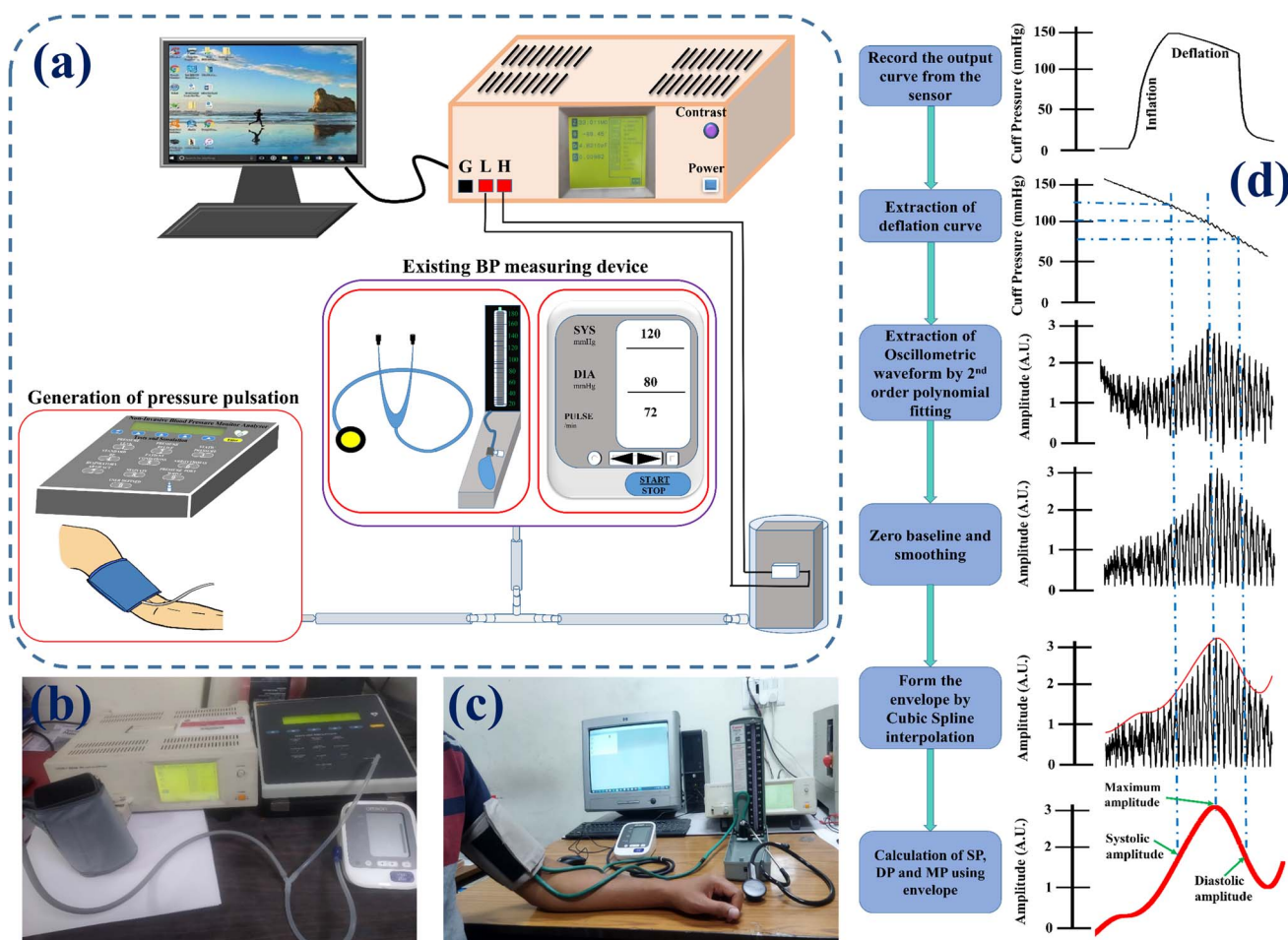
Fig. 3 (a) The schematic illustration of the experimental set-up for BP monitoring. (b and c) Photographs of the experimental set-up using NIBP and the human body providing a pulse to the sensor. (d) The pictorial representation of the MAA approach used to determine BP values.
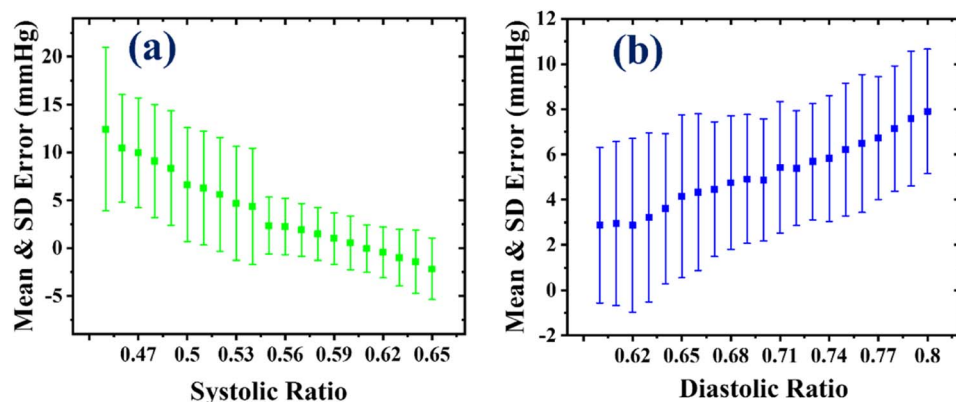

Fig. 4 The mean and SD error variation at different (a) systolic and (b) diastolic characteristic ratios.

encompassing both the range of values and the corresponding mean values along with their standard deviations, is given in Table 1. Among them, four participants were on medication for hypertension and diabetes. We implemented several preventive measures to ensure accurate BP measurement during the procedure: (i) the subject's posture and hand position relative to their heart adjusted following the established protocol; (ii) all volunteers were instructed to refrain from speaking and engaging in any physiological movements.[55] For all participants, the developed sensor traced the oscillometric waveform very well, and using the aforementioned approach (MAA), the SP, DP and MP values were calculated. The BP values were

Table 1 Participant age, height and weight with their ranges and mean ± SD values

Parameters	Range	Mean value with SD
Age (years)	20–63	32 ± 10
Height (cm)	149–185	168 ± 8
Weight (kg)	44–96	71 ± 11

computed for the entire cohort of 130 participants, of which the values of 114 volunteers were within the low, normal, and high normal ranges. The values of the remaining 16 participants indicated varying conditions, including hypotension and grade I hypertension. Among these 16 individuals, 2 were diagnosed with isolated systolic hypotension, 10 exhibited grade I hypertension and 3 were diagnosed with isolated grade II and III diastolic hypertension. The categories of BP based on the systolic and diastolic values are given in Table ST1.†

The correlation and Bland–Altman (B&A) plots were used to compare the values obtained from the sensor with the reference values acquired from the BP device. It is important to note that the BP device solely provides systolic (SP) and diastolic (DP) values without offering mean arterial pressure (MP). Consequently, a facile formula was used to estimate the MP value for the BP device, *i.e.*, MAP = 1/3 (SP) + 2/3 (DP). The correlation plot illustrates the relationship between the measured and reference values. These correlation plots are depicted in Fig. 5(a)–(c). The Pearson correlation coefficients, denoted as R^2, for SP, DP, and MP were 0.97, 0.95, and 0.93, respectively. These coefficients signify a strong linear relationship between the sensor results and the reference values. Furthermore, the sensor accurately estimated the SP value, while it slightly overestimated the DP and MP values, as demonstrated in Fig. 5(a)–(c).

On the other hand, the Bland–Altman (B&A) plot is a graphical representation that illustrates the variation between two
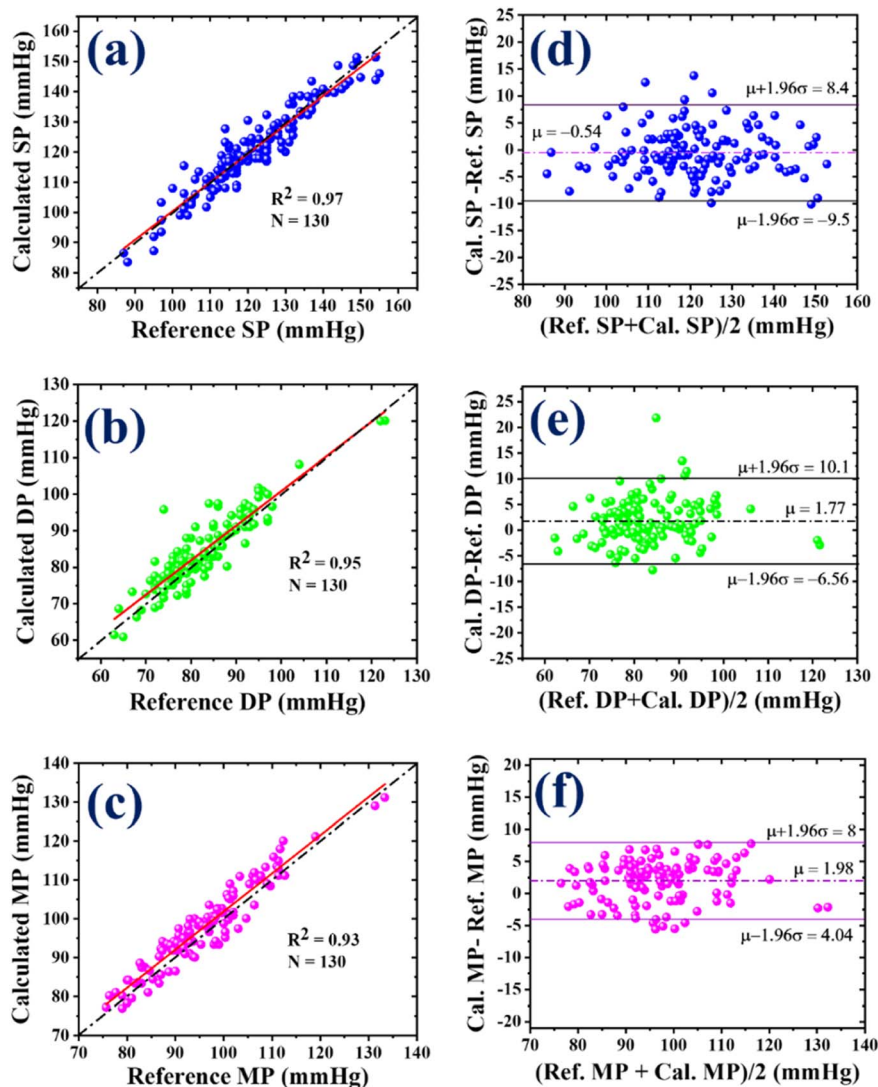

Fig. 5 The correlation plots of (a) SP, (b) DP, and (c) MP for $N = 130$. (d–f) The Bland–Altman plots for mean error (μ) and SD (σ) in SP, DP, and MP, respectively, indicate that 95% of the measurements were within the limit of agreement.

simultaneously measured BP values and is plotted against the average of both measurements. In this plot, the difference between the BP values obtained from the two devices is taken on the *y*-axis, while the *x*-axis represents the average of the measurements from both devices. This plot is utilized to assess and quantify the level of agreement between the measured BP values. The mean (μ) and standard deviation (σ) of the difference between the two measurements are computed to establish a statistical limit. According to the B&A analysis, it is recommended that 95% of the measurements should fall within the range of $\mu \pm 1.96(\sigma)$.[56] Fig. 5(d)–(f) present the error with standard deviation (SD) along with the limit of agreement for systolic pressure (SP), diastolic pressure (DP), and mean pressure (MP), respectively. These plots provide valuable insights into the agreement between the measurements obtained from the developed sensor and the reference device. In the case of SP, the mean error (μ) was −0.54 mmHg with an SD (σ) of 4.56 mmHg, and the limit of agreement was −9.5 to 8.4 mmHg. As seen in Fig. 5(d), 95% of the SP measurements were within the range of agreement. The mean error (μ) for DP was 1.77 mmHg, and the SD (σ) was 4.25 mmHg. The range of agreement for DP was −6.56 to 10.1 mmHg, encompassing approximately 96% of the DP measurements, as shown in Fig. 5(e). For MP, the values of μ and σ were 1.98 and 3.07 mmHg, respectively. As shown in Fig. 5(f), 96% of the MP measurements were in the range of agreement, *i.e.*, from 4.04 to 8 mmHg. Based on the correlation and B&A plots, it can be concluded that there was a good level of agreement between the results obtained from the developed sensor and those from the reference device.

To validate a non-invasive blood pressure (BP) measurement device, a universal standard AAMI/ESH/ISO has been established. According to this protocol, the clinical validation of a BP measuring device requires a minimum of 85 participants. All participants must be older than 12 years, and the male-to-female ratio should be equal to or greater than 30%. Under the AAMI/ESH/ISO protocol, there are two pass criteria for a device to fulfill: (i) at least 85% of the total measurements should have less than 10 mmHg error, and (ii) the overall or average error for the entire measurement cohort should be less than 5 mmHg for the mean and less than 8 mmHg for SD.[54] These pass criteria serve as benchmarks to determine the accuracy and reliability of a BP measuring device under the AAMI/ESH/ISO protocol. For the first criterion, a scatter plot was plotted for SP, DP and MP with a 10 mmHg error limit, as depicted in Fig. 6(a). The results indicate that 97% of SP and DP measurements were within the 10 mmHg error range (denoted by a dashed-dotted line), while 100% of MP measurements fulfilled this criterion, as represented in Fig. 6(a). The average and SD error ($\mu \pm \sigma$) were computed for the obtained SP, DP and MP values for the second pass criterion. The values of $\mu \pm \sigma$ for SP, DP, and MP were −0.5 ± 4.6, −1.8 ± 4.2, and −1.9 ± 3.1, respectively, as demonstrated in Fig. 6(b). These results demonstrate that the developed sensor accurately measures BP from the human artery and fulfills the requirements set by the universal standard. Therefore, it can be concluded that the developed sensor can replace the sensors in existing BP devices and provide better BP measurements.

In addition to BP, pulse rate (PR) was calculated using the same approach to find the SP, DP and MP values. The obtained
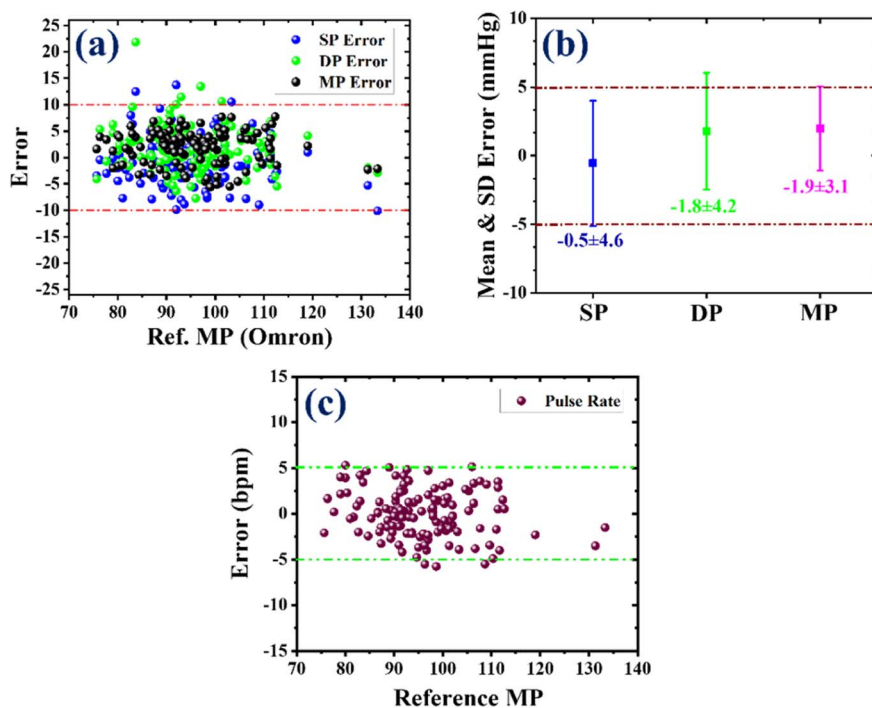

Fig. 6 The pass criterion of AAMI/ESH/ISO standard. (a) The errors in the computed SP, DP and MP values, as per the first criterion. (b) The mean errors with standard deviation (SD) of the SP, DP, and MP values, as per the second criterion. (c) The errors in the sensor reading of the human pulse rate *versus* the OMRON BP device.
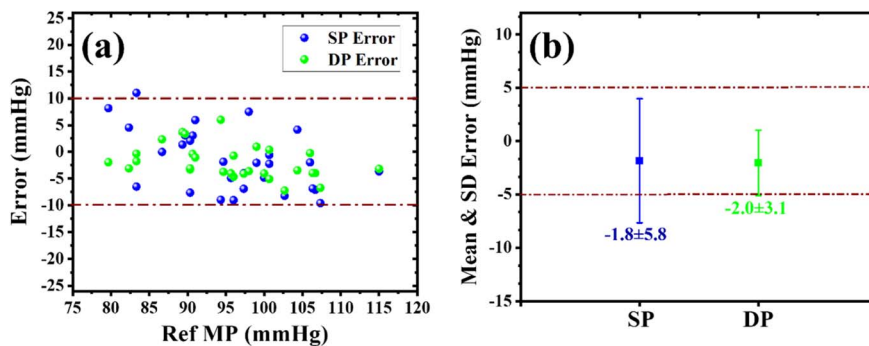
Fig. 7 (a) Scatter plot and (b) the mean and SD error plot between values obtained from the sensor and a mercury-based sphygmomanometer according to the AAMI/ESH/ISO Universal standard.

PR values from the sensor were compared with those from the reference device (OMRON BP device), and the error between them was determined. As seen in Fig. 6(c), nearly 98% of the total PR values were within the error range of 5 bpm (beats per minute), which signifies that the developed sensor accurately measures PR.

After clinical validation of the developed sensor using the OMRON BP device, the sensor results were further compared with the gold standard, a mercury-based sphygmomanometer (a reference device). In this study, 30 volunteers participated (with informed consent), including 24 males and 6 females. Their age, height, and weight ranges were from 22 to 59 years, 152 to 181 cm, 50 to 97 kg, respectively. The photograph of the experimental set-up is shown in Fig. 3(c). While using the reference device, the BP was obtained by listening to the Korotkoff sound using a stethoscope, and the BP values for the developed sensor were calculated using the same procedure described previously. Among the participants, one volunteer was found to have grade I hypertension. Fig. S3(a) and (b)† illustrate the correlation plots for SP and DP values. The corresponding Pearson correlation coefficients for SP and DP were 0.91 and 0.90, indicating a strong linear relationship between the sensor results and reference values. In the B&A plot for SP, as shown in Fig. S3(c),† the average error and SD were −1.83 and 5.8 mmHg, and nearly 97% of measurements were in the agreement range. Similarly, for DP, the values of μ and σ were −2.0 and 3.1 mmHg, and nearly 97% of measurements were within the limit of agreement, as demonstrated in Fig. S3(d).† To evaluate if the sensor results fulfill the two pass criteria of the universal standard, the scatter plot and average SD error of the SP and DP values were plotted, as presented in Fig. 7. As seen in Fig. 7(a), nearly 97% of SP and 100% of DP measurements were within the 10 mmHg error range. The average and SD error for SP was −1.8 ± 5.8 and that for DP was −2.0 ± 3.1, as shown in Fig. 7(b). In this study, the number of participants or sample size was less than the recommended protocol, which typically requires a sample size of 85. However, despite the smaller sample size, the sensor accurately measured BP and validated the universal standard defined by AAMI/ESH/ISO. Further studies with a larger sample set would provide evidence of sensor accuracy and reliability.

The developed sensor successfully met all the criteria specified by the universal standard when compared with an existing BP device and the gold-standard mercury-based sphygmomanometer. Furthermore, the sensor demonstrated good agreement with the OMRON BP device in measuring pulse rate. Thus, the obtained BP values from the developed sensor can easily evaluate whether a person has normal blood pressure, hypertension, or hypotension, which is the primary objective of this study. Additionally, the traced OMW features provide valuable information about conditions related to the participant's heart function, such as sinus arrhythmia, bradycardia, and tachycardia. Hence, the developed sensor can monitor various aspects of cardiovascular health. Moreover, the high flexibility and wearable nature of the developed sensor make it a promising candidate for integration into healthcare monitoring devices, which would expand its applications beyond BP monitoring.

4. Conclusion

In this study, we have improved the critical parameters of a previously developed capacitive pressure sensor to enable its use in BP monitoring. This was achieved by incorporating baking powder in the previously developed PDMS-DIW dielectric layer.[29] The resulting device showed excellent performance with an improved sensitivity of 0.021 Pa^{-1}, an extremely low detection limit of 1 Pa, a quick reaction and recovery with a time of 100 ms, and high operational stability. To clinically validate the developed sensor, a clinical trial involving 160 participants across a wide range of ages, heights and weights was conducted. The sensor traced the OMW for all participants with different BP conditions. Systolic and diastolic values were computed from the obtained OMW by employing specific characteristic ratios calibrated against an NIBP simulator, which served as a reference device. To assess sensor accuracy, we used correlation, Bland–Altman, and scatter plots to compare the sensor results with the values obtained from two reference devices: the OMRON BP device and the gold-standard mercury-based sphygmomanometer. Additionally, average or mean with standard deviation (SD) errors were also calculated for all measurements. These analyses were performed in accordance with the AAMI/ESH/ISO standard. The developed sensor exhibited excellent performance in accurately measuring BP and successfully met all the criteria specified by the universal

standard when compared to the existing BP device and the gold-standard mercury-based sphygmomanometer. Furthermore, the sensor accurately provided the pulse rate (PR) and agreed well with the OMRON BP device. Thus, the obtained BP values from the developed sensor can effectively determine whether an individual has normal BP, hypertension, or hypotension, which is the primary objective of this study. Moreover, the high flexibility, wearable nature and excellent performance of the developed sensor make it a promising candidate for integration into healthcare monitoring devices toward extending its applications beyond BP monitoring.

Data availability

The datasets used and/or analyzed during the current study available from the corresponding author on reasonable request.

Conflicts of interest

There are no conflicts to declare.

Acknowledgements

References

1 M. Choi and S. J. Lee, Oscillometry-Based Blood Pressure Estimation Using Convolutional Neural Networks, *IEEE Access*, 2022, **10**, 56813–56822, DOI: **10.1109/ACCESS.2022.3177539**.

2 A. Abiri, E. F. Chou, C. Qian, J. Rinehart and M. Khine, Intra-Beat Biomarker for Accurate Continuous Non-Invasive Blood Pressure Monitoring, *Sci. Rep.*, 2022, **12**(1), 1–13, DOI: **10.1038/s41598-022-19096-6**.

3 H. Tanaka, A. Mito, H. Hirano, Z. Soh, R. Nakamura, N. Saeki, M. Kawamoto, Y. Higashi, M. Yoshizumi and T. Tsuji, Estimation of Arterial Viscosity Based on an Oscillometric Method and Its Application in Evaluating the Vascular Endothelial Function, *Sci. Rep.*, 2019, **9**, 2609, DOI: **10.1038/s41598-019-38776-4**.

4 B. Lee, J. H. Jeong, J. Hong and Y. H. Park, Correlation Analysis of Human Upper Arm Parameters to Oscillometric Signal in Automatic Blood Pressure Measurement, *Sci. Rep.*, 2022, **12**(1), 1–11, DOI: **10.1038/s41598-022-24264-9**.

5 F. D. Fuchs and P. K. Whelton, High Blood Pressure and Cardiovascular Disease, *Hypertension*, 2020, 285–292, DOI: **10.1161/HYPERTENSIONAHA.119.14240**.

6 S. Allender, P. Scarborough, V. Peto, M. Rayner, J. Leal, R. Luengo-Fernandez, and A. Gray, *European Cardiovascular Disease Statistics*, 2008.

7 L. Y. Ma, W. W. Chen, R. L. Gao, L. S. Liu, M. L. Zhu, Y. J. Wang, Z. S. Wu, H. J. Li, D. F. Gu, Y. J. Yang, Z. Zheng and S. S. Hu, China Cardiovascular Diseases Report 2018:

8 An Updated Summary, *J. Geriatr. Cardiol.*, 2020, **17**(1), 1, DOI: **10.11909/J.ISSN.1671-5411.2020.01.001**.

8 S. Zhang; C. Wang; L. Ding; L. Zhang; *et al.*, A Flexible Bifunctional Sensor Based on Porous Copper Nanowire@IonGel Composite Films for High-Resolution Stress/Deformation Detection. J. C.-J. of M.; 2020, undefined. pubs.rsc.org.

9 Y. Zang, F. Zhang, C. A. Di and D. Zhu, Advances of Flexible Pressure Sensors toward Artificial Intelligence and Health Care Applications, *Mater. Horiz.*, 2015, **2**(2), 140–156, DOI: **10.1039/C4MH00147H**.

10 W. Asghar, F. Li, Y. Zhou, Y. Wu, Z. Yu, S. Li, D. Tang, X. Han, J. Shang, Y. Liu and R. W. Li, Piezocapacitive Flexible E-Skin Pressure Sensors Having Magnetically Grown Microstructures, *Adv. Mater. Technol.*, 2020, **5**(2), 1900934, DOI: **10.1002/ADMT.201900934**.

11 B. Wang, T. Shi, Y. Zhang, C. Chen, Q. Li and Y. Fan, Lignin-Based Highly Sensitive Flexible Pressure Sensor for Wearable Electronics, *J. Mater. Chem. C*, 2018, **6**(24), 6423–6428, DOI: **10.1039/C8TC01348A**.

12 W. Yang, N. W. Li, S. Zhao, Z. Yuan, J. Wang, X. Du, B. Wang, R. Cao, X. Li, W. Xu, Z. L. Wang and C. Li, A Breathable and Screen-Printed Pressure Sensor Based on Nanofiber Membranes for Electronic Skins, *Adv. Mater. Technol.*, 2018, **3**(2), 1700241, DOI: **10.1002/ADMT.201700241**.

13 Bijender and A. Kumar, Broadening the Utilization of Flexible and Wearable Pressure Sensors for the Monitoring of Health and Physiological Activities, *Biomed. Mater. Diagn. Devices*, 2023, **1**, 1–13, DOI: **10.1007/S44174-023-00069-W**.

14 Bijender and A. Kumar, Recent Progress in the Fabrication and Applications of Flexible Capacitive and Resistive Pressure Sensors, *Sens. Actuators, A*, 2022, **344**, 113770, DOI: **10.1016/J.SNA.2022.113770**.

15 Y. Ding, J. Yang, C. R. Tolle and Z. Zhu, Flexible and Compressible PEDOT:PSS@Melamine Conductive Sponge Prepared via One-Step Dip Coating as Piezoresistive Pressure Sensor for Human Motion Detection, *ACS Appl. Mater. Interfaces*, 2018, **10**(18), 16077–16086, DOI: **10.1021/ACSAMI.8B00457/ASSET/IMAGES/LARGE/AM-2018-00457K_0007.JPEG**.

16 S. Kumar, S. Yadav and A. Kumar, Oscillometric Waveform Evaluation for Blood Pressure Devices, *Biomed. Eng. Adv.*, 2022, **4**, 100046, DOI: **10.1016/J.BEA.2022.100046**.

17 Y. Xiong, Y. Shen, L. Tian, Y. Hu, P. Zhu, R. Sun and C. P. Wong, A Flexible, Ultra-Highly Sensitive and Stable Capacitive Pressure Sensor with Convex Microarrays for Motion and Health Monitoring, *Nano Energy*, 2020, **70**, 104436, DOI: **10.1016/J.NANOEN.2019.104436**.

18 T. Dinh, T. Nguyen, H. P. Phan, N. T. Nguyen, D. V. Dao and J. Bell, Stretchable Respiration Sensors: Advanced Designs and Multifunctional Platforms for Wearable Physiological Monitoring, *Biosens. Bioelectron.*, 2020, **166**, 112460, DOI: **10.1016/J.BIOS.2020.112460**.

19 F. Zhang, K. Yang, Z. Pei, Y. Wu, S. Sang, Q. Zhang and H. Jiao, A Highly Accurate Flexible Sensor System for Human Blood Pressure and Heart Rate Monitoring Based

on Graphene/Sponge, *RSC Adv.*, 2022, **12**(4), 2391–2398, DOI: **10.1039/D1RA08608A**.

20 X. Wang, Z. Liu and T. Zhang, Flexible Sensing Electronics for Wearable/Attachable Health Monitoring, *Small*, 2017, **13**(25), 1602790, DOI: **10.1002/SMLL.201602790**.

21 C. Wang, C. Wang, Z. Huang and S. Xu, Materials and Structures toward Soft Electronics, *Adv. Mater.*, 2018, **30**(50), 1801368, DOI: **10.1002/ADMA.201801368**.

22 A. Nathan, A. Ahnood, M. T. Cole, S. Lee, Y. Suzuki, P. Hiralal, F. Bonaccorso, T. Hasan, L. Garcia-Gancedo, A. Dyadyusha, S. Haque, P. Andrew, S. Hofmann, J. Moultrie, D. Chu, A. J. Flewitt, A. C. Ferrari, M. J. Kelly, J. Robertson, G. A. J. Amaratunga and W. I. Milne, Flexible Electronics: The next Ubiquitous Platform, *Proc. IEEE*, 2012, **100**, 1486–1517, DOI: **10.1109/JPROC.2012.2190168**.

23 D. Jiang, Y. Wang, B. Li, C. Sun, Z. Wu, H. Yan, L. Xing, S. Qi, Y. Li, H. Liu, W. Xie, X. Wang, T. Ding, Z. Guo, D. Jiang, Y. Wang, B. Li, C. Sun, S. Qi, H. Yan, L. Xing, Y. Li, H. Liu, W. Xie, X. Wang, T. Ding and Z. Guo, Flexible Sandwich Structural Strain Sensor Based on Silver Nanowires Decorated with Self-Healing Substrate, *Macromol. Mater. Eng.*, 2019, **304**(7), 1900074, DOI: **10.1002/MAME.201900074**.

24 X. Tang, C. Wu, L. Gan, T. Zhang, T. Zhou, J. Huang, H. Wang, C. Xie and D. Zeng, Multilevel Microstructured Flexible Pressure Sensors with Ultrahigh Sensitivity and Ultrawide Pressure Range for Versatile Electronic Skins, *Small*, 2019, **15**(10), 1804559, DOI: **10.1002/SMLL.201804559**.

25 Y. Ding, T. Xu, O. Onyilagha, H. Fong and Z. Zhu, Recent Advances in Flexible and Wearable Pressure Sensors Based on Piezoresistive 3D Monolithic Conductive Sponges, *ACS Appl. Mater. Interfaces*, 2019, **11**(7), 6685–6704, DOI: **10.1021/ACSAMI.8B20929/ASSET/IMAGES/LARGE/AM-2018-20929N_0017.JPEG**.

26 J. Bae, Y. Hwang, S. J. Park, J. H. Ha, H. J. Kim, A. Jang, J. An, C. S. Lee and S. H. Park, Study on the Sensing Signal Profiles for Determination of Process Window of Flexible Sensors Based on Surface Treated PDMS/CNT Composite Patches, *Polymers*, 2018, **10**(9), 951, DOI: **10.3390/POLYM10090951**.

27 H. Li, K. Wu, Z. Xu, Z. Wang, Y. Meng and L. Li, Ultrahigh-Sensitivity Piezoresistive Pressure Sensors for Detection of Tiny Pressure, *ACS Appl. Mater. Interfaces*, 2018, **10**(24), 20826–20834, DOI: **10.1021/ACSAMI.8B03639/ASSET/IMAGES/LARGE/AM-2018-03639T_0004.JPEG**.

28 S. Kumar, Bijender, S. Yadav and A. Kumar, Flexible Microhyperboloids Facets Giant Sensitive Ultra-Low Pressure Sensor, *Sens. Actuators, A*, 2021, **328**, 112767, DOI: **10.1016/J.SNA.2021.112767**.

29 Bijender and A. Kumar, Flexible and Wearable Capacitive Pressure Sensor for Blood Pressure Monitoring, *Sens. Bio-Sens. Res.*, 2021, **33**, 100434, DOI: **10.1016/J.SBSR.2021.100434**.

30 Bijender and A. Kumar, One-Rupee Ultrasensitive Wearable Flexible Low-Pressure Sensor, *ACS Omega*, 2020, **5**(27), 16944–16950, DOI: **10.1021/ACSOMEGA.0C02278/ASSET/IMAGES/LARGE/AO0C02278_0007.JPEG**.

31 J. C. Yang, J. O. Kim, J. Oh, S. Y. Kwon, J. Y. Sim, D. W. Kim, H. B. Choi and S. Park, Microstructured Porous Pyramid-Based Ultrahigh Sensitive Pressure Sensor Insensitive to Strain and Temperature, *ACS Appl. Mater. Interfaces*, 2019, **11**(21), 19472–19480, DOI: **10.1021/ACSAMI.9B03261/ASSET/IMAGES/LARGE/AM-2019-032613_0002.JPEG**.

32 Bijender and A. Kumar, Effect of Porosity and Microstructure on the Functionality of Capacitive Pressure Sensors, *Mater. Chem. Phys.*, 2023, **304**, 127872, DOI: **10.1016/J.MATCHEMPHYS.2023.127872**.

33 W. Wang, Y. Zheng, X. Jin, Y. Sun, B. Lu, H. Wang, J. Fang, H. Shao and T. Lin, Unexpectedly High Piezoelectricity of Electrospun Polyacrylonitrile Nanofiber Membranes, *Nano Energy*, 2019, **56**, 588–594, DOI: **10.1016/J.NANOEN.2018.11.082**.

34 J. Zhou, Y. Gu, J. Lu, L. Xu, J. Zhang, D. Wang and W. Wang, An Ultra-Strong Non-Pre-Irradiation and Self-Recoverable Mechanoluminescent Elastomer, *Chem. Eng. J.*, 2020, **390**, 124473, DOI: **10.1016/J.CEJ.2020.124473**.

35 S. M. Villa, M. Maturi, T. Santaniello, L. Migliorini, E. Locatelli, M. Comes Franchini and P. Milani, Quantitative Spectral Electromechanical Characterization of Soft Piezoelectric Nanocomposites, *Sens. Actuators, A*, 2021, **332**, 113196, DOI: **10.1016/J.SNA.2021.113196**.

36 V. Narayan Thakur and J. In Han, Triboelectric Nanogenerator for Smart Traffic Monitoring and Safety, *J. Ind. Eng. Chem.*, 2023, **124**, 89–101, DOI: **10.1016/J.JIEC.2023.04.028**.

37 V. K. S. Hsiao, S. F. Leung, Y. C. Hsiao, P. K. Kung, Y. C. Lai, Z. H. Lin, K. N. Salama, H. N. Alshareef, Z. L. Wang and J. H. He, Photo-Carrier Extraction by Triboelectricity for Carrier Transport Layer-Free Photodetectors, *Nano Energy*, 2019, **65**, 103958, DOI: **10.1016/J.NANOEN.2019.103958**.

38 T. Zhong, M. Zhang, Y. Fu, Y. Han, H. Guan, H. He, T. Zhao, L. Xing, X. Xue, Y. Zhang and Y. Zhan, An Artificial Triboelectricity-Brain-Behavior Closed Loop for Intelligent Olfactory Substitution, *Nano Energy*, 2019, **63**, 103884, DOI: **10.1016/J.NANOEN.2019.103884**.

39 Z. Wang, L. Zhang, J. Liu, H. Jiang and C. Li, Flexible Hemispheric Microarrays of Highly Pressure-Sensitive Sensors Based on Breath Figure Method, *Nanoscale*, 2018, **10**(22), 10691–10698, DOI: **10.1039/C8NR01495G**.

40 J. Heikenfeld, A. Jajack, J. Rogers, P. Gutruf, L. Tian, T. Pan, R. Li, M. Khine, J. Kim, J. Wang and J. Kim, Wearable Sensors: Modalities, Challenges, and Prospects, *Lab Chip*, 2018, **18**(2), 217–248, DOI: **10.1039/C7LC00914C**.

41 S. Chen, K. Jiang, Z. Lou, D. Chen, G. Shen, S. Chen, D. Chen, Z. Lou, G. Z. Shen and K. Jiang, Recent Developments in Graphene-Based Tactile Sensors and E-Skins, *Adv. Mater. Technol.*, 2018, **3**(2), 1700248, DOI: **10.1002/ADMT.201700248**.

42 Q. Yu, P. Zhang and Y. Chen, Human Motion State Recognition Based on Flexible, Wearable Capacitive Pressure Sensors, *Micromachines*, 2021, **12**(10), 1219, DOI: **10.3390/MI12101219**.

43 M. Maturi, V. Vetri Buratti, G. Casula, E. Locatelli, L. Sambri, A. Bonfiglio and M. Comes Franchini, Surface-Stabilization

of Ultrathin Gold Nanowires for Capacitive Sensors in Flexible Electronics, *ACS Appl. Nano Mater.*, 2021, **4**(9), 8673, DOI: **10.1021/acsanm.1c01849**.

44 Y. Joo, J. Byun, N. Seong, J. Ha, H. Kim, S. Kim, T. Kim, H. Im, D. Kim and Y. Hong, Silver Nanowire-Embedded PDMS with a Multiscale Structure for a Highly Sensitive and Robust Flexible Pressure Sensor, *Nanoscale*, 2015, **7**(14), 6208–6215, DOI: **10.1039/C5NR00313J**.

45 M. Farman, N. Surendra, R. Prajesh, A. K. Upadhyay, P. Kumar and E. Thouti, All-Polydimethylsiloxane-Based Highly Flexible and Stable Capacitive Pressure Sensors with Engineered Interfaces for Conformable Electronic Skin, *ACS Appl. Mater. Interfaces*, 2023, **15**(28), 34195–34205, DOI: **10.1021/ACSAMI.3C04227/SUPPL_FILE/AM3C04227_SI_005.MP4**.

46 S. Masihi, M. Panahi, D. Maddipatla, A. J. Hanson, A. K. Bose, S. Hajian, V. Palaniappan, B. B. Narakathu, B. J. Bazuin and M. Z. Atashbar, Highly Sensitive Porous PDMS-Based Capacitive Pressure Sensors Fabricated on Fabric Platform for Wearable Applications, *ACS Sens.*, 2021, **6**(3), 938–949, DOI: **10.1021/ACSSENSORS.0C02122/ASSET/IMAGES/LARGE/SE0C02122_0007.JPEG**.

47 S. Chen, B. Zhuo and X. Guo, Large Area One-Step Facile Processing of Microstructured Elastomeric Dielectric Film for High Sensitivity and Durable Sensing over Wide Pressure Range, *ACS Appl. Mater. Interfaces*, 2016, **8**(31), 20364–20370, DOI: **10.1021/ACSAMI.6B05177/ASSET/IMAGES/LARGE/AM-2016-05177P_0005.JPEG**.

48 B.-Y. Lee, J. Kim, H. Kim, C. Kim and S.-D. Lee, Low-Cost Flexible Pressure Sensor Based on Dielectric Elastomer Film with Micro-Pores, *Sens. Actuators, A*, 2016, **240**, 103–109, DOI: **10.1016/j.sna.2016.01.037**.

49 S. Baek, H. Jang, S. Y. Kim, H. Jeong, S. Han, Y. Jang, D. H. Kim and H. S. Lee, Flexible Piezocapacitive Sensors Based on Wrinkled Microstructures: Toward Low-Cost Fabrication of Pressure Sensors over Large Areas, *RSC Adv.*, 2017, **7**(63), 39420–39426, DOI: **10.1039/C7RA06997A**.

50 J. C. Yang, J. O. Kim, J. Oh, S. Y. Kwon, J. Y. Sim, D. W. Kim, H. B. Choi and S. Park, Microstructured Porous Pyramid-Based Ultrahigh Sensitive Pressure Sensor Insensitive to Strain and Temperature, *ACS Appl. Mater. Interfaces*, 2019, **11**(21), 19472–19480, DOI: **10.1021/ACSAMI.9B03261/ASSET/IMAGES/LARGE/AM-2019-032613_0002.JPEG**.

51 D. Zhu, S. Handschuh-Wang and X. Zhou, Recent Progress in Fabrication and Application of Polydimethylsiloxane Sponges, *J. Mater. Chem. A*, 2017, **15**, 16467–16497, DOI: **10.1039/c7ta04577h**.

52 J. Qin, L. J. Yin, Y. N. Hao, S. L. Zhong, D. L. Zhang, K. Bi, Y. X. Zhang, Y. Zhao and Z. M. Dang, Flexible and Stretchable Capacitive Sensors with Different Microstructures, *Adv. Mater.*, 2021, **33**(34), 2008267, DOI: **10.1002/ADMA.202008267**.

53 E. S. Hosseini, M. Chakraborty, J. Roe, Y. Petillot and R. S. Dahiya, Porous Elastomer Based Wide Range Flexible Pressure Sensor for Autonomous Underwater Vehicles, *IEEE Sens. J.*, 2022, **22**(10), 9914–9921, DOI: **10.1109/JSEN.2022.3165560**.

54 G. S. Stergiou, P. Palatini, R. Asmar, J. P. Ioannidis, A. Kollias, P. Lacy, R. J. McManus, M. G. Myers, G. Parati, A. Shennan, J. Wang and E. O'Brien, Recommendations and Practical Guidance for Performing and Reporting Validation Studies According to the Universal Standard for the Validation of Blood Pressuremeasuring Devices by TheAssociation for the Advancement OfMedical Instrumentation/European Society OfHypertension/InternationalOrganization for Standardization (AAMI/ESH/ISO), *J. Hypertens.*, 2019, **37**(3), 459–466, DOI: **10.1097/HJH.0000000000002039**.

55 G. Livadiotis, D. J. McComas, M. A. Dayeh, A. E. Kaloyeros, Y. Pan, J. Goff, F. A. Jové, A. Boraschi, A. Spiegelberg, F. Karimi, K. Graf, A. Fallahi, E. Neufeld, N. Kuster and V. Kurtcuoglu, The Effect of Body Position Change on Noninvasively Acquired Intracranial Pulse Waves, *Physiol. Meas.*, 2023, **44**(3), 035014, DOI: **10.1088/1361-6579/ACC3D6**.

56 D. Giavarina, Understanding Bland Altman Analysis, *Biochem. Med.*, 2015, **25**(2), 141–151, DOI: **10.11613/BM.2015.015**.